X-ray Variations at the Orbital Period from Cygnus X-1 in the High/Soft State

Bram Boroson

Smithsonian Astrophysical Observatory Mail Stop 83 Cambridge, MA 02138

bboroson@cfa.harvard.edu

and

Saeqa Dil Vrtilek

Smithsonian Astrophysical Observatory Mail Stop 67 Cambridge, MA 02138

svrtilek@cfa.harvard.edu

Received _____; accepted _____

ABSTRACT

Orbital variability has been found in the X-ray hardness of the black hole candidate Cygnus X-1 during the soft/high X-ray state using light curves provided by the Rossi X-ray Timing Explorer's All Sky Monitor. We are able to set broad limits on how the mass-loss rate and X-ray luminosity vary between the hard and soft states. The folded light curve shows diminished flux in the soft X-ray band at $\phi = 0$ (defined as the time of of the superior conjunction of the X-ray source). Models of the orbital variability provide slightly superior fits when the absorbing gas is concentrated in neutral clumps and better explain the strong variability in hardness. In combination with the previously established hard/low state dips, our observations give a lower limit to the mass loss rate in the soft state ($\dot{M} < 2 \times 10^{-6}$ $M_\odot$ yr^{-1}) than the limit in the hard state ($\dot{M} < 4 \times 10^{-6}$ $M_\odot$ yr-1). Without a change in the wind structure between X-ray states, the greater mass-loss rate during the low/hard state would be inconsistent with the increased flaring seen during the high-soft state.

Subject headings: black hole binaries: individual (Cyg X-1), X-rays: binaries

1. Introduction

X-ray binary systems in which the compact object is thought to be a black hole from dynamical or X-ray timing evidence (Black Hole Candidates, or BHC, see Remillard & McClintock 2006) are often found to shift between spectral states distinguished by hardness and intensity at X-rays and γ-rays (Grove et al. 1998). This class of source comprises several objects of which the BHC Cygnus X-1 is a member (Grebenev et al. 1993).

Cygnus X-1 is unusual in that it is persistently bright in X-rays and has a high mass donor star, HDE 226868, with mass 18-40 $M_\odot$ (Ziólkowski 2005; Tarasov et al. 2003; Caballero-Nieves et al. 2009) and accretes primarily from a stellar wind. In contrast most BHC are transients (hence cannot be revisited in coordinated observing campaigns) and have low mass companions that accrete via Roche lobe overflow. The compact object in Cygnus X-1 has a mass of 7-20 $M_\odot$ (Herrero et al. 1995; Ziólkowski 2005). No pulsations or bursts have ever been detected. The strong stellar wind of the donor star, and its complex interaction with the compact object, can be studied through the UV P-cygni lines and X-ray absorption (refs).

The binary orbital period of $P = 5.6$ days was first discoved by Bolton (1972) and refined by Brocksopp et al. (1999b) using radial velocities of the O-star. Brocksopp et al. found P = 5.599829±0.000016d, with an epoch of the inferior conjuction of the O-star of To=41874.207±0.009MJD and we use their values. The X-ray phases computed from this ephemeris are accurate to 0.007 in phase through the end of the ASM data set, which is sufficient for our purposes.

Gies et al. (2003) used the results of a four year spectroscopic monitoring of the Hα emission strength of HDE226868, the noncompact companion to Cyg X-1, to conclude that the changes in X-ray state are driven by changes in $\dot{M}$, the mass-loss rate through the wind. Gies et al. find that $\dot{M}$ is lower during the soft/high state and suggest that in this state,

the X-rays ionize the wind to a greater extent and slow its acceleration. As a result, the black hole can accrete more matter and the total X-ray luminosity increases.

Spectra obtained with the *Chandra* High Energy Transmission Gratings suggest that the stellar wind increases in density towards the compact object. This "focused wind" may cause increased X-ray absorption at orbital phases from $\phi = 0.7 - 0.9$. Miller et al. (2005) found that at $\phi = 0.76$ the X-ray shows strong absorption lines, consistent with this scenario. Further observations of X-ray spectra during this phase interval have returned varying results. Schulz et al. (2002) suggest some X-ray lines may have P Cygni profiles at $\phi = 0.93$, although Marshall et al. (2001) did not find such features at $\phi = 0.84$. Hanke et al. (2009) pointed out that the previous observations of the focused wind were made at times when the RXTE ASM count rate varied by nearly a factor of 3.

The behavior of lines in the UV does not support the focused wind picture. The wind-formed UV P Cygni absorption gradually decreases as the compact object moves towards the line of sight, whereas a focused wind might be expected to cause a sharp increase in the absorption (Vrtilek et al. 2008). The general trend of the P Cygni line variation is consistent with the Hatchett-McCray effect (Hatchett & McCray 1977), in which an orbiting X-ray source removes ions from a stellar wind. The UV spectrum has been observed with *IUE* (Dupree et al. 1978, Treves et al. 1980, van Loon et al. 2001), which has shown that absorption in the P Cygni lines of N V, C IV, and Si IV diminishes near $\phi = 0.5$. Recent analyses of Hubble Space Telescope Imaging Spectrograph (HST STIS) observations of Cyg X-1 during the soft/high state provided more detailed diagnostics of the structure of the stellar wind (Vrtilek et al. 2008, Geis et al. 2008).

The X-ray light curve of Cyg X-1 shows intensity dips near $\phi = 0$. This was first observed with Copernicus (Mason et al. 1974, Treves et al. 1980) and Ariel 5 (Holt et al. 1979). Power spectra of a 100 day time series collected with WATCH (Priedhorsky, Brandt,

& Lund 1995) showed a dip of $\approx 20\%$ near $\phi = 0$. In an analysis of 2 years of RXTE/ASM data of Cyg X-1, Wen et al. (1999) found variability at the 5.6 day orbital period during the X-ray low/hard state, but no evidence of orbital periodicity during the high/soft state. Similar results were found by Brocksopp et al. (1999a), who also studied simultaneous orbital variability in optical, IR, and radio light curves. Absorption of X-rays by a stellar wind from the companion star can reproduce the observed X-ray orbital modulations in the hard state. However, the RXTE ASM observations covered ≈ 900 days and only one soft/high state at the time of the Wen et al. analysis. As the RXTE ASM data have accumulated, the Cyg X-1 data set has been revisited for analysis. Balucińska-Church et al. (2000) identified discrete dipping events from a number of X-ray observatories including the RXTE ASM and showed that their distribution in the hard/low state peaks near $\phi = 0$ with a secondary peak near $\phi = 0.6$. Pointed observations with RXTE over the course of Cyg X-1's orbit suggest that there are at least two different kinds of X-ray dips in Cyg X-1 (Feng & Cui 2002). Dips can either preferentially affect the low-energy spectrum or can decrease the spectrum in a nearly energy-independent manner.

Lachowicz et al. (2006) and Ibragimov, Zdziarski, & Poutanen (2007) found evidence in the RXTE ASM data for a superorbital period and a beat period between the orbital and superorbital periods. Lachowicz et al. (2006) looked for but did not find evidence for orbital periodicity in the soft/high period. Simultaneous radio observations did, however, show the 5.6 d orbital period. Dong, Wang, & Xue (2007) reported evidence for variability at the 5.6 d period during the soft state, in addition to periodicities at 1.0 ± 0.2 d and 18.0 ± 3.0 d. They did not evaluate the significance of these periodicities, however, nor did they examine the fractional variability or folded light curves of these variations.

The RXTE ASM data set now covers more than 4000 days and about 5 soft/high states. A larger data set should be more sensitive to weak variability and may display states

which the source enters into less frequently.

Here we show convincing evidence for the 5.6 d period during the soft state by using the more extensive data set accumulated by RXTE and by examining the variability of the X-ray colors, that is, the ratio of X-ray flux between different energy bands. We examine the nature of this orbital variability and use the observations to set limits on how the stellar wind may change between the soft and hard states.

2. Observations

The Rossi X-ray Timing Explorer (RXTE) (Bradt, Rothschild, & Swank 1993), launched in 1995, includes an All Sky Monitor (ASM, Levine et al. 1996). The ASM contains three scanning shadow cameras (SSCs) with total effective area of 90 cm^2.

In addition to the ASM, RXTE contains a Proportional Counter Array (PCA, Jahoda et al. 1996) and High Energy X-ray Timing Experiment (HEXTE, Rothschild et al. 1998). The PCA has an effective area of ~ 6500 cm^2 and HEXTE has an effective area of ~ 1000 cm^{-2}, allowing spectra in the 2–200 keV range to be obtained with a variety of timing modes down to $\sim 1\mu$s.

2.1. RXTE ASM

The RXTE ASM Products Database provides light curves and intensities in the 1.5-3, 3-5, and 5-12 keV bands ("colors") for ≈ 350 sources. We use the Definitive Products version of the data that has been processed at MIT. In the resulting time series, there are often two measurements that occur at exactly the same time. This is because two of the SSCs have overlapping fields of view and can provide independent measurements. For our

analysis, when this occurs we average the two measurements. For the ASM observatons of Cyg X-1, 70% of the measurements carry a unique time stamp. The error bars on the light curves and colors are based on counting statistics convolved with a 3% systematic error, as estimated by the RXTE ASM team from Crab pulsar measurements.

We divide the ASM observations into periods of soft/high and consider the remainder of the period to be hard/low (Table 1, Figure 1). There are short intervals that appear similar to the soft/high states that we do not single out, but treat as part of the remaining hard/low state. We choose the time interval of the Soft 3 period to correspond with the interval chosen by Lachowicz et al. (2006).

2.2. RXTE PCA/HEXTE Observations

To supplement our analysis of RXTE ASM data, we also use pointed RXTE PCA/HEXTE observations. We consider the data set of 202 observations from 1999 through 2004 examined in Wilms et al. (2006). These observations were scheduled biweekly for lengths of ~ 5 ksec. Wilms et al. fit the spectra between 3 and 200 keV to three models: a broken power law with exponential cutoff, the Comptonization model of Titarchuk (1994), and the Comptonization model of Coppi (1999). These fits were used to explore the hard and soft states, and led to the conclusion that there is a continuum between these states. However, the fits have not previously been used to investigate the 5.6 day orbital period.

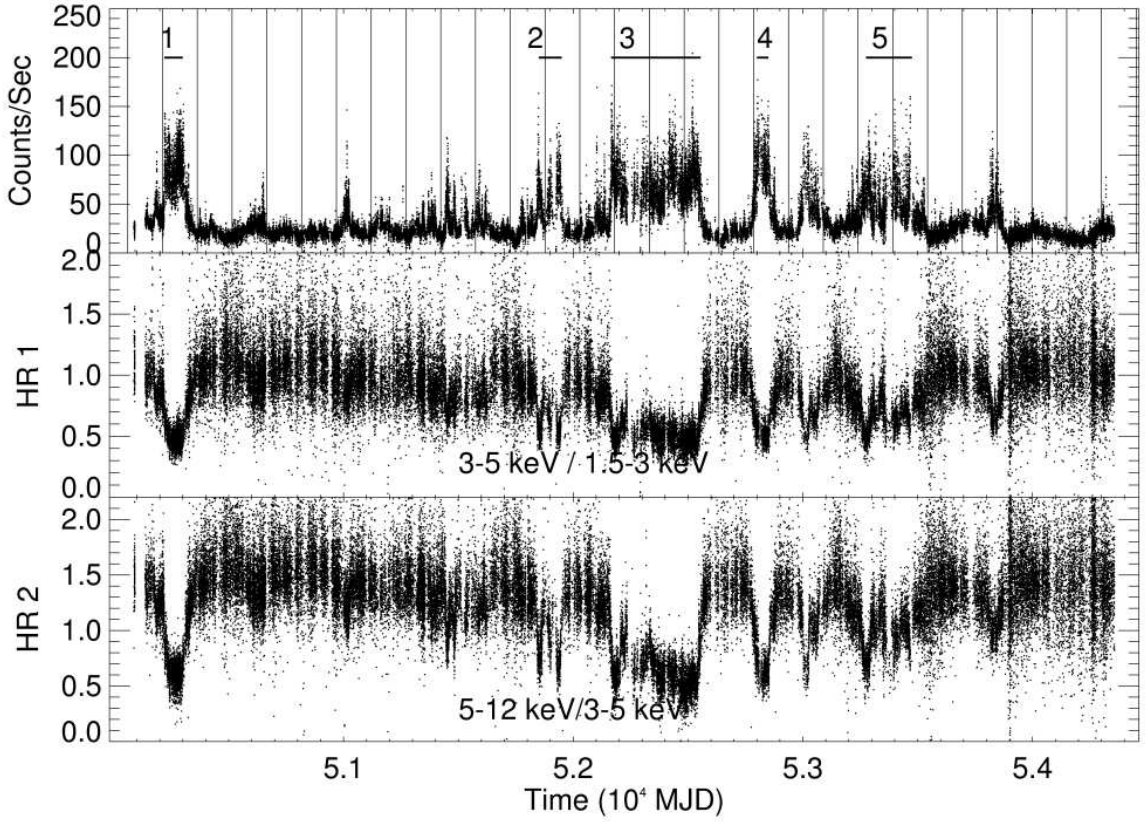

Fig. 1.— The RXTE ASM light curves and hardness ratios over a 4270 day interval from the start of the ASM observations. We show the light curve of total counts, the hardness ratios HR 1 and HR 2, and the light curves in the 1-3 keV, 3-5, and 5-12 keV ranges. Horizontal bars in top panels show the definitions of the Soft 1, 2, 3, 4, and 5 states. Vertical bars in the top left panel show times of superorbital phase 0 according to the ephemeris of Lachowicz et al. 2006.

3. Dip Variability

3.1. Soft State Periodicty with the ASM

We apply the Lomb Normalized Periodogram (Scargle 1982) and the Analysis of Variance (ANOVA, Davies 1991) methods to search for periodicity in the RXTE ASM observations of Cyg X-1.

The Lomb Normalized Periodogram is a generalization of the Fourier power spectrum to unevenly sampled data. In the case of evenly sampled time series, the Lomb Normalized Periodogram is identical to the power spectrum. When we apply this periodogram to the hardness ratio HR 1 (as defined in Figure 1) during the Soft 3 period, we find a peak power of 73 at a period of 5.61 days and a power of 47 in the neighboring bin at 5.59 days. We eliminated points with HR 1 below 0 or above 3, as negative hardness ratios are not physically meaningful and large hardness ratios result from division by count rates near 0 and carry large uncertainties. This only eliminated 2 of 6038 data points in the soft state. We show the Lomb Normalized Periodogram for each of the 5 soft states we have identified in Figure 2.

For a power spectrum of uniformly sampled data, normalized so that the white noise level is 1, the probability of a signal level s would be $\exp(-s)$. A LNP power of 73 corresponds therefore to a false alarm probability of 2×10^{-32}. However, the signal at 5.6 days does not appear against white noise, but instead against a continuum strongest at low frequencies. Examination of the distribution of powers shows that they obey a distribution closer to $\exp(-s/4)$, which would imply a false alarm probability of only $\approx 10^{-8}$, implying a much lower significance of the signal.

Application of ANOVA to the HR 1 ratio in the Soft 3 period gives a probability of 5×10^{-23} that variation at 5.6 days is random. For this test, we used 16 phase bins. As

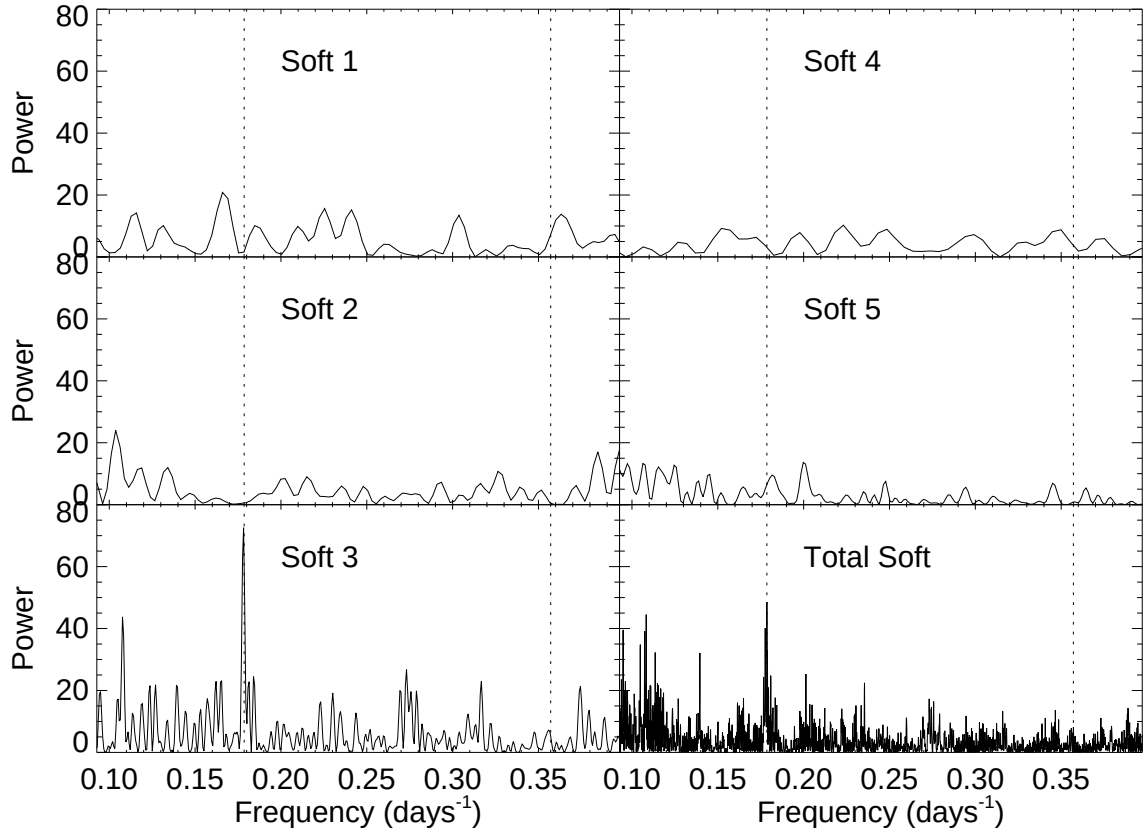

Fig. 2.— The Lomb Normalized Periodogram of the H1 hardness ratio of Cygnus X-1, as observed by RXTE ASM during the 5 soft periods we have selected. The frequencies corresponding to a 5.6 day orbital period and its first harmonic are marked with vertical dotted lines.

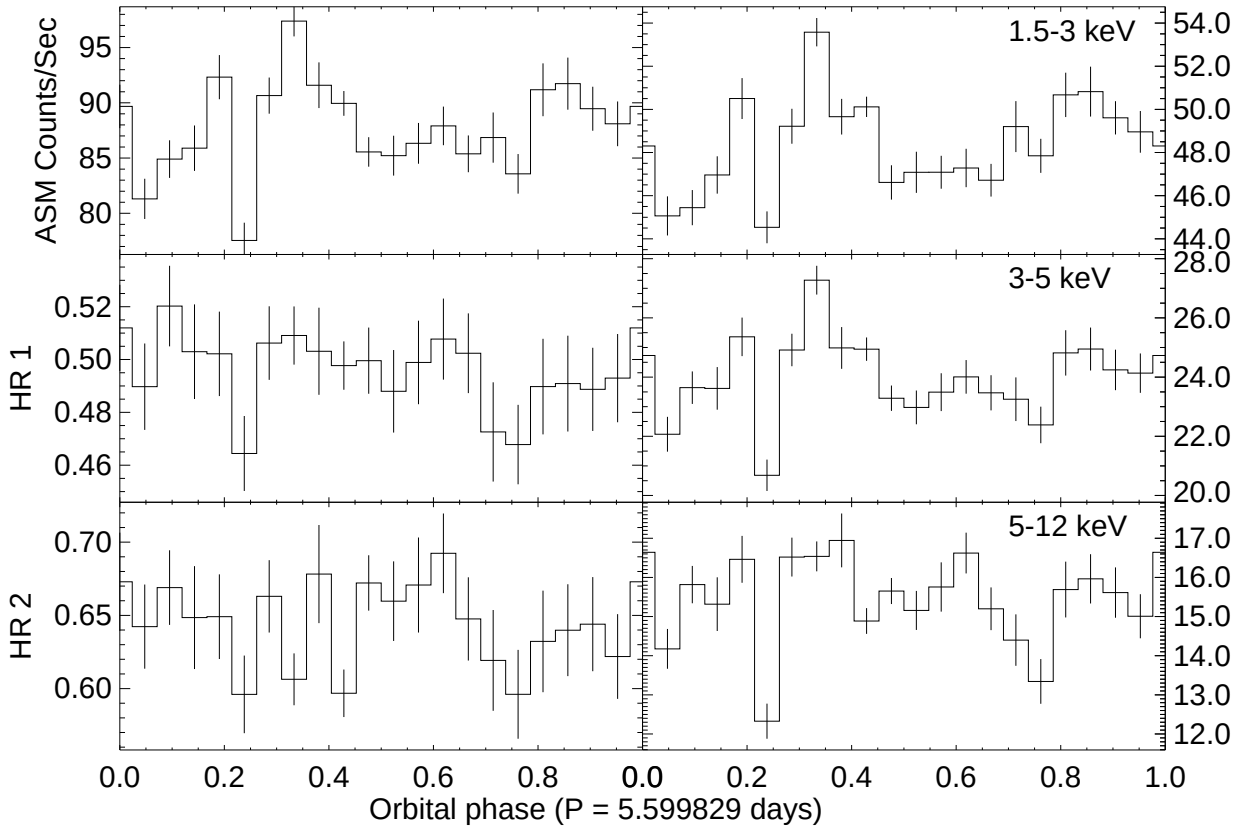

Fig. 3.— Light curves and hardness ratios folded with the 5.6 day Cyg X-1 orbital period during the Soft 1 period.

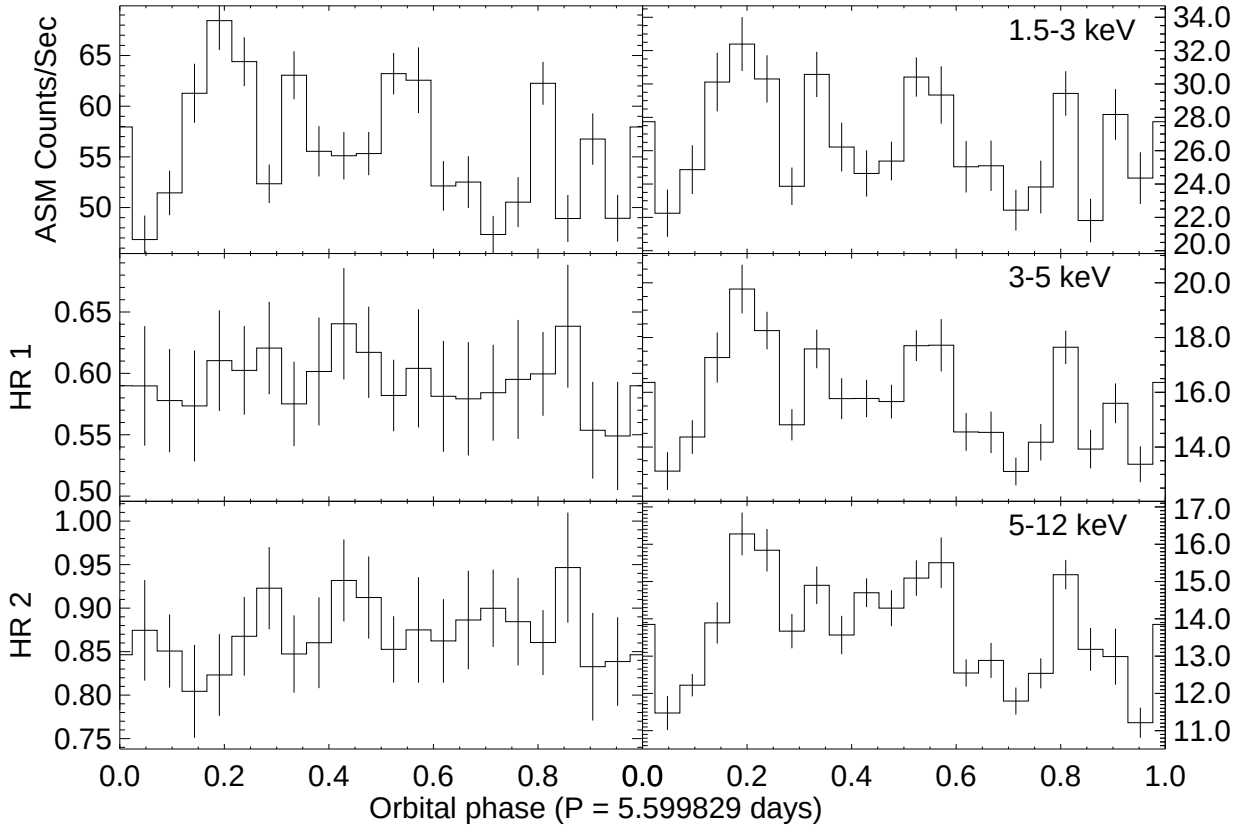

Fig. 4.— As in Figure 3, for the Soft 2 period.

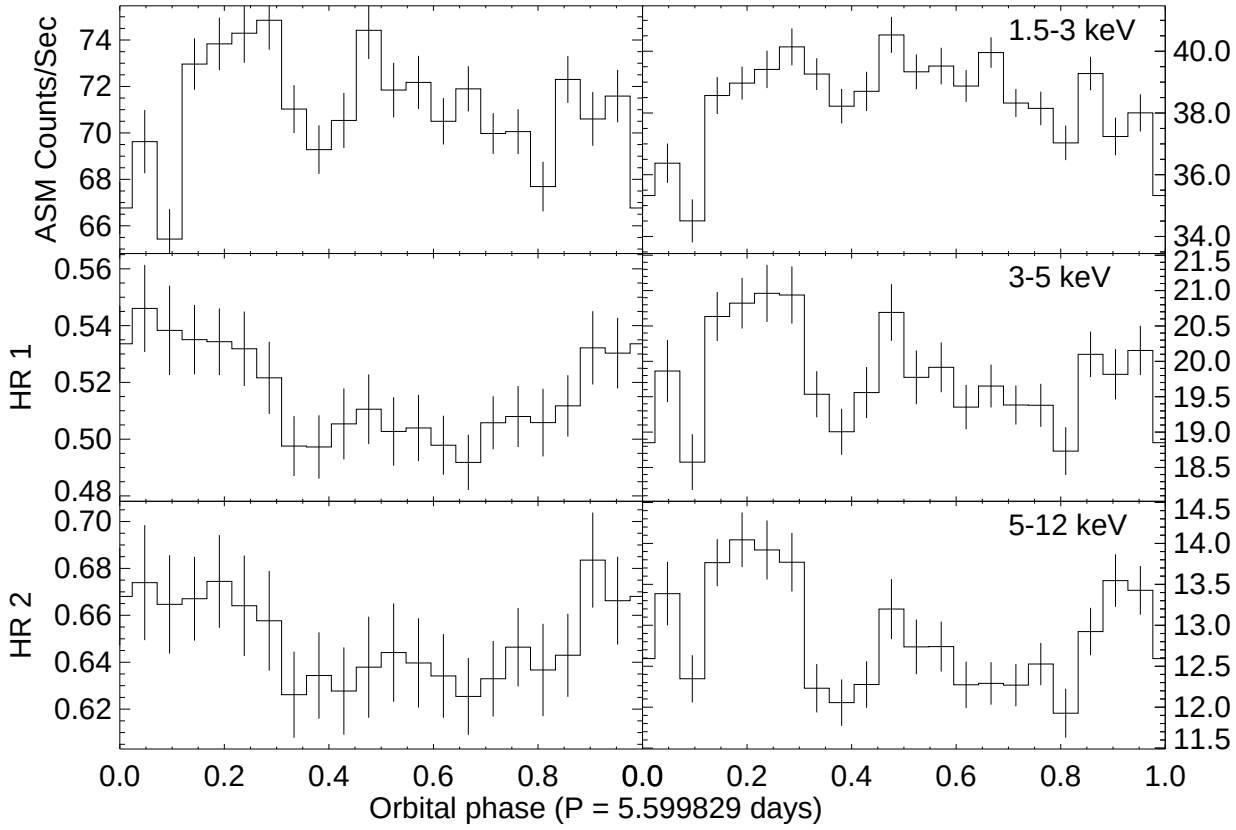

Fig. 5.— As in Figure 3, for the Soft 3 period.

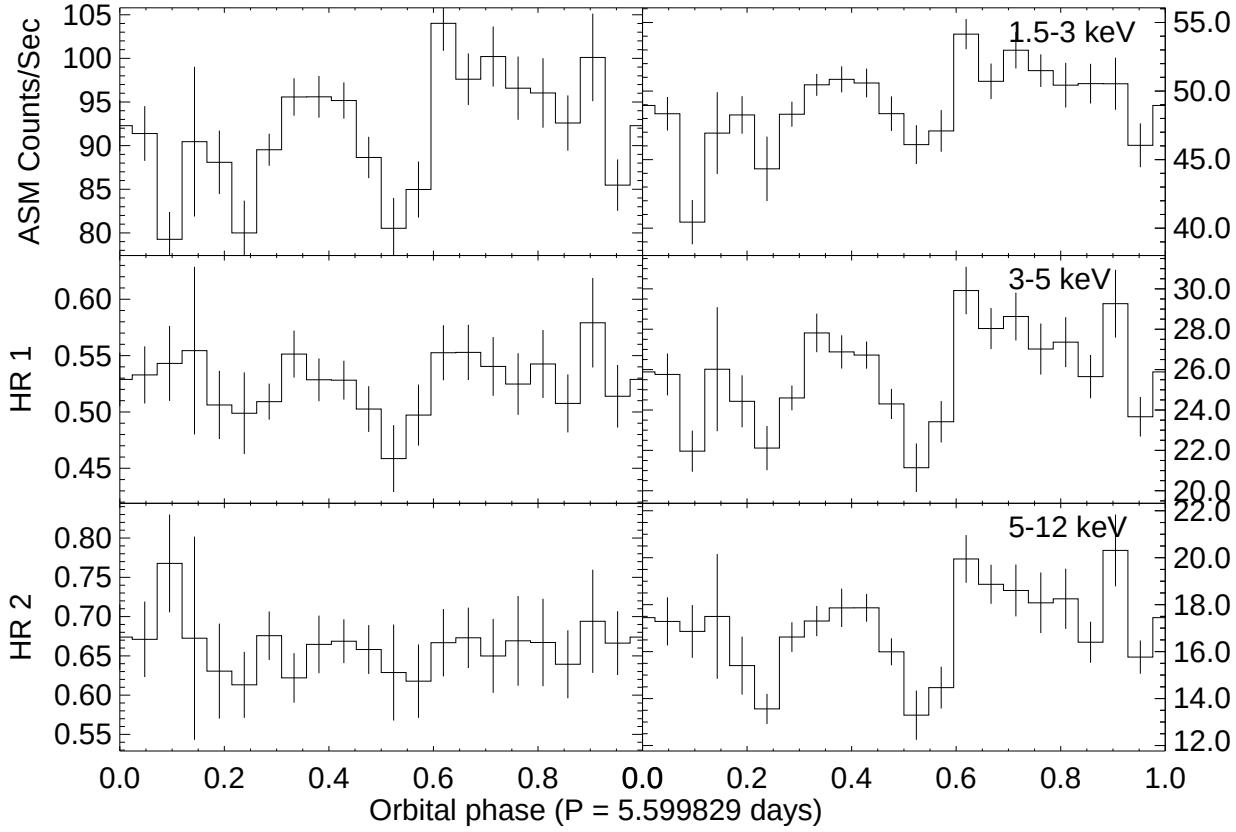

Fig. 6.— As in Figure 3, for the Soft 4 period.

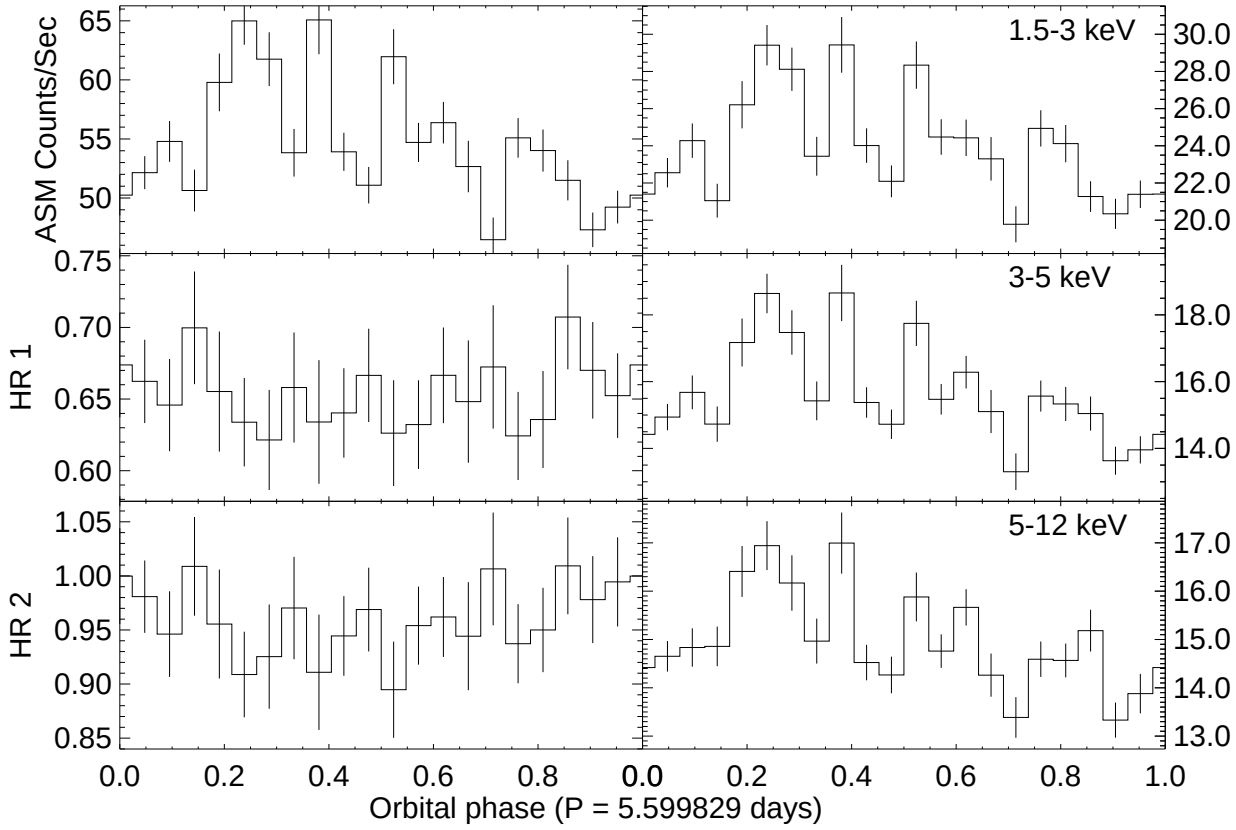

Fig. 7.— As in Figure 3, for the Soft 5 period.

with the power spectral methods, the ANOVA method may return a false positive in a test for periodicity if the power spectrum contains a significant continuum component, and the significance given by this method may be an overestimate.

We have found a clear orbital variation in the hardness ratio HR 1, but not in the individual energy bands in the same period ("Soft 3"). The count rates in the individual energy bands are more variable on all timescales than HR1. For example, during Soft 3, the χ^2_ν fit for a constant count rate in the 1.5-3 keV range is 62 with 6037 degrees of freedom. The χ^2_ν fit for a constant HR 1 is 7.1. As a result of this greater non-orbital variability, it may be harder to detect any orbital variation in the actual count rates than in HR1, which may increase near $\phi = 0$ with the absorbing column, but which may be less affected by flares than the count rates.

If the Soft 3 orbital variation is $n\sigma$ significant, then scaling from the duration of the observations, the Soft 1 and Soft 2 variability should be $\approx 0.4\sigma$ significant and the Soft 5 variability should be $\approx 0.7\sigma$ significant. However, the rms variability in HR1 is 50% higher for Soft 5, so that we might expect only $\approx 0.5\sigma$ significance in the orbital variations. The rms variation in the 3 X-ray bands and 2 hardness ratios are within a factor of 2 for all the Soft states, except for HR2 in Soft 2, which appears anomalously high.

We also tested whether the HR1 variability seen during the Soft 3 period would appear significant in shorter intervals of that same period. Lomb Normalized Periodograms of the first or middle 200 days of Soft 3 show no significant variation at the orbital period, though the power spectrum of the last 200 days shows a peak as great as for the total Soft 3 period. There was no significant variation in HR1 in the first 100 days of Soft 3, or in days 190 through 290, but within the last 100 days the power spectral peak reached 65. For the last 50 day interval in Soft 3, the power spectral peak is 47, but no significant peak was seen for the first or second 50 day periods, or another 50 day period near the end of Soft 3. Intervals

of 200 days, 100 days, and 50 days are identical to the lengths of the Soft 1, Soft 4, and Soft 2 periods, respectively. In conclusion, it is possible that orbital variability as strong as that seen during the Soft 3 state could occur during all soft states but went undetected by RXTE/ASM during the shorter Soft 1, Soft 2, Soft 4, and Soft 5 states.

In Figures 3 to 7, we present light curves and hardness ratios during the Soft states 1 to 5, folded with the 5.6 day binary period.

3.2. Individual dips seen with the RXTE ASM

We have demonstrated with both power spectra and epoch folding methods that the hardness ratio and count rate show the 5.6 day orbital periodicity during the Soft 3 state. However, previous studies of dips in the hard state have suggested that discrete dips may occur at any phase, but may simply be more likely to occur near $\phi = 0$.

Cyg X-1 shows both dips in which the spectrum hardens (color dips) and also monochromatic dips (count dips) in which the count rate diminishes but the color does not change appreciably (Feng & Cui 2002). We thus have 4 classes of dips to compare: color and count dips in the soft and hard states. We choose criteria to define these dips.

3.2.1. Color dips in the soft state

Color dips in the hard state were already considered by Balucińska-Church et al. (2000). They selected as dips those observations with hardness ratios HR1$>$ 2.0 or HR2$>$ 2.5. We adjust these criteria to the changed spectrum during the soft state.

If we choose as dips those data points with HR1/$\overline{\mathrm{HR1}} > 1.96$, where $\overline{\mathrm{HR1}}$ is the mean hardness ratio, we find only 14 observations to count as dips in the Soft 3 state. From §3.1

we know that HR1 varies with the orbital period, so a less restrictive criterion should select individual observations (dips) with some preference for orbital phase. We thus choose some constant $k < 1$ and select dips based on $\mathrm{HR1}/\overline{\mathrm{HR1}} > 1.96k$. The results, shown in Figure 8, demonstrate that the strongest dips defined by HR1 color cluster near $\phi = 0$. Weaker dips depend less strongly on phase.

For comparison, we show a histogram of color dips in the hard state in Figure 9. As there is more data for the hard state than for the Soft 3 state, this plot has less scatter. It shows more clearly the trend that stronger dips are more likely to occur near $\phi = 0$.

3.2.2. Count dips in the hard state

Dips selected by low count rate (count dips) are less frequent in the soft state and show no obvious orbital clustering. Count dips in the hard state cluster with phase similarly to color dips (Figure 10). To select dips based on count rate, we choose an interval for the constant b and select ASM observations with count rate $\mathrm{CR} = b\overline{\mathrm{CR}}$. We find that stronger count-selected dips are more likely to occur near $\phi = 0$.

3.3. Hard State Variability with the RXTE PCA/HEXTE

While the 202 pointed RXTE PCA/HEXTE observations fit to models by Wilms et al. (2006) cover the Soft 3 period, they are not extensive enough to show the orbital variability in the soft state.

However, the pointed observations suffice to show the orbital variability in the hard state, already demonstrated with RXTE ASM observations. The broken power law fits of Wilms et al., include the hydrogen column density N_{H} as a free parameter. In Figure 4 we

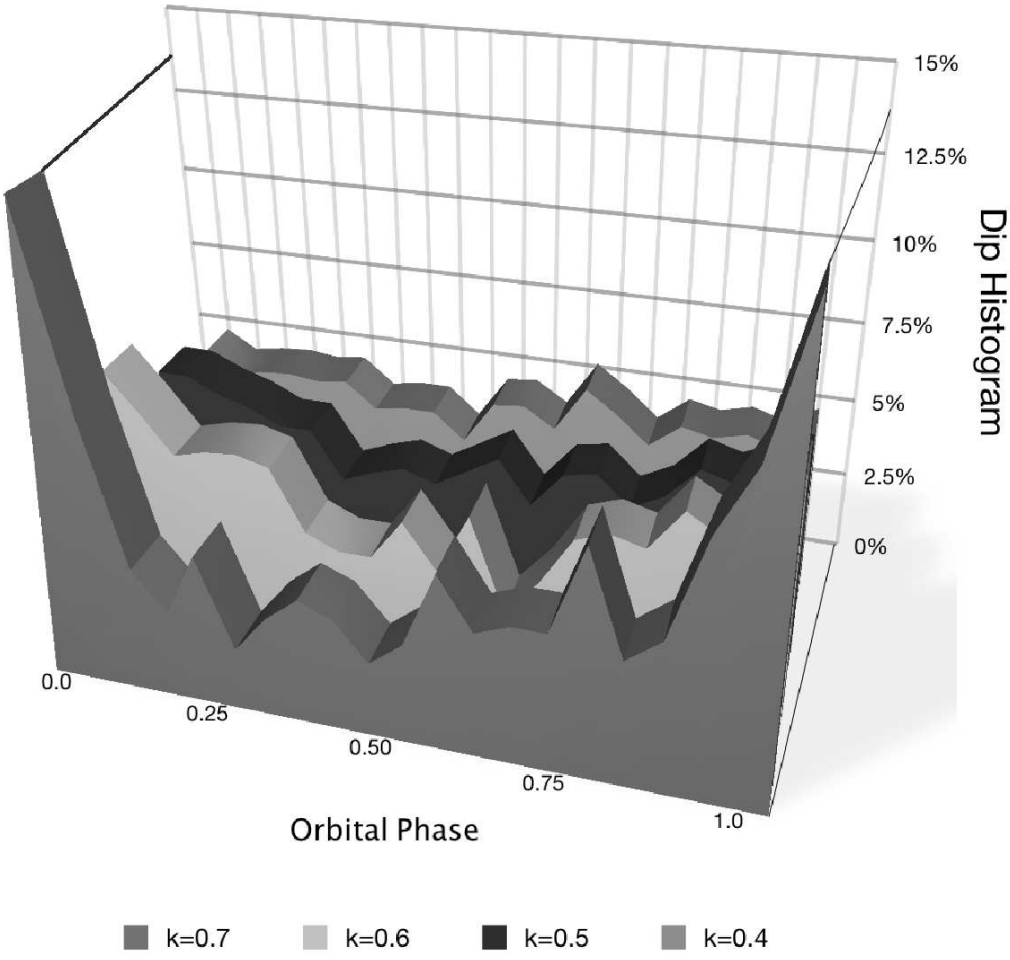

Fig. 8.— Histograms of color dips versus orbital phase in the "Soft 3" state. The number of dips at each phase interval are divided by the total number of dips. There are 20 phase intervals from 0.0 to 1.0. From bottom to top, we show histograms of dips defined by $\mathrm{HR1}/\overline{\mathrm{HR1}} > 1.96k$, where $\overline{\mathrm{HR1}}$ is the mean hardness ratio in the Soft 3 state.

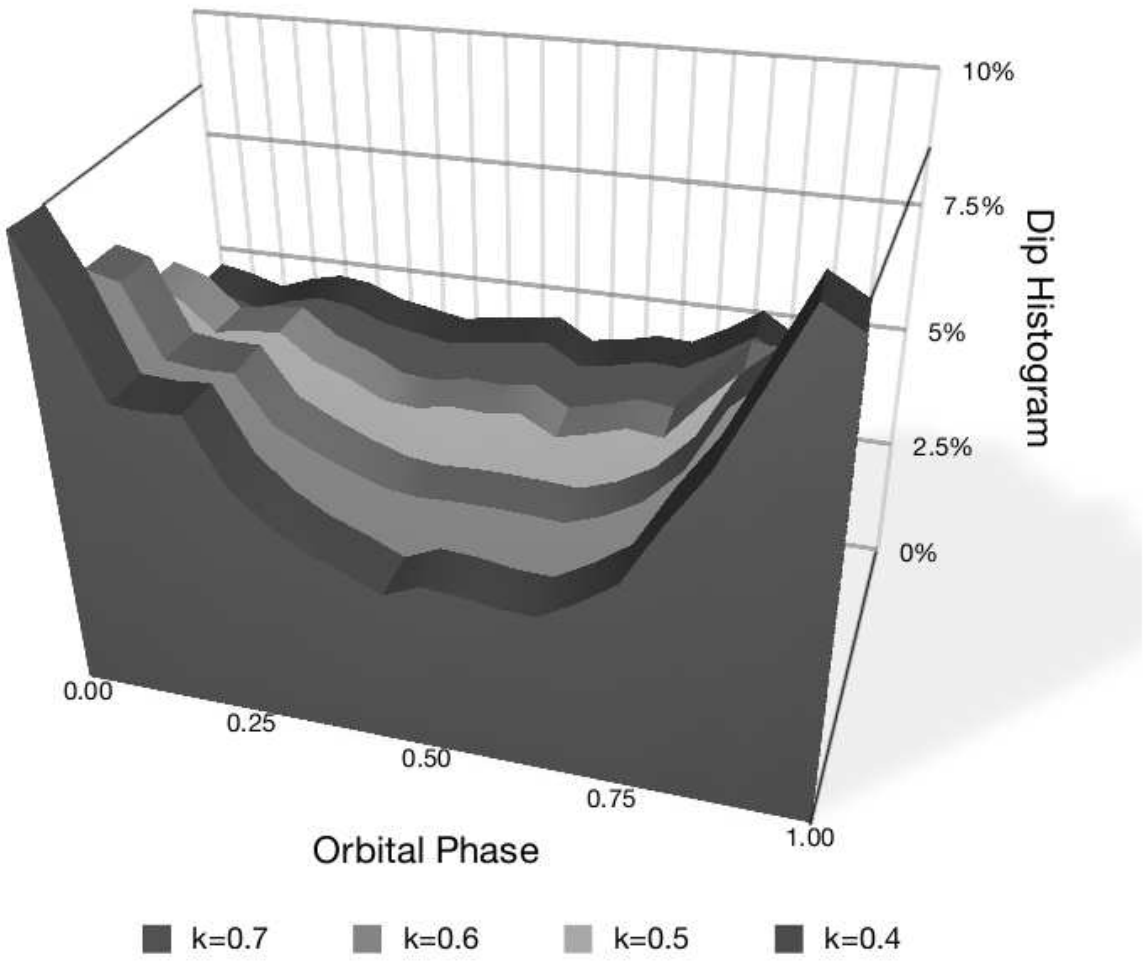

Fig. 9.— Histograms of color dips versus orbital phase in the Hard state, for different depths of the dips. The number of dips at each phase interval are divided by the total number of dips. We show stacked histograms of dips defined by $\mathrm{HR1}/\overline{\mathrm{HR1}} > 1.96k$, where $\overline{\mathrm{HR1}}$ is the mean hardness ratio in the Hard state.

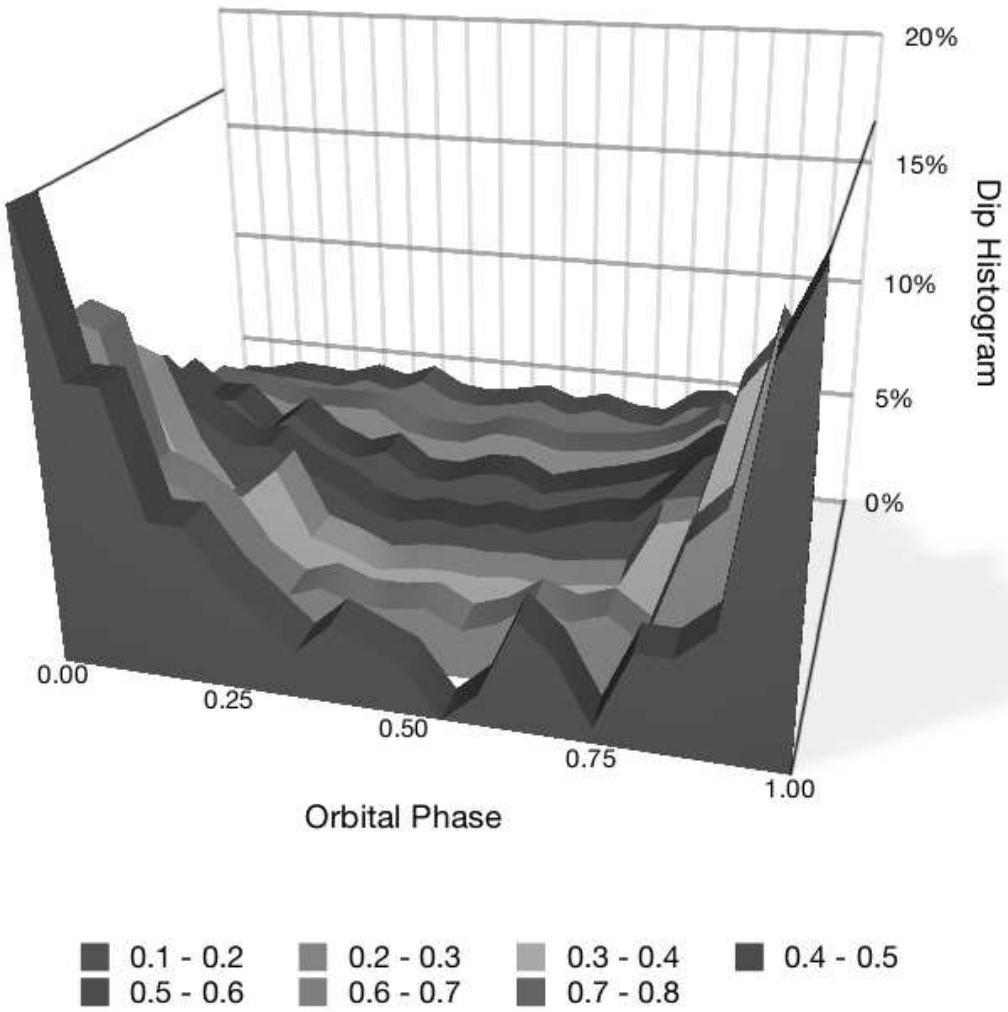

Fig. 10.— Histograms of count dips versus orbital phase in the RXTE ASM observations of Cygnus X-1 in the hard state. The number of dips at each phase interval are divided by the total number of dips. From bottom to top, we show histograms of dips defined by $0.1 < \mathrm{CR}/\overline{\mathrm{CR}} < 0.2$, $0.2 < \mathrm{CR}/\overline{\mathrm{CR}} < 0.3$, etc. up to $0.7 < \mathrm{CR}/\overline{\mathrm{CR}} < 0.8$, where CR is the count rate and $\overline{\mathrm{CR}}$ is the mean count rate in the hard state.

show the fitted value of this parameter during the hard state folded over the 5.6 day period, where we have defined the hard state by F(5-10)/F(2-5) > 0.3, where F(5-10) is the 5-10 keV flux according to the model and F(2-5) is the 2-5 keV flux. Eliminating observations that have $N_{\rm H} = 0$ leaves 133 data points. Applying ANOVA, we find a false alarm probability 4×10^{-8} for a periodicity at 5.6 days. If instead we examine F(5-10)/F(2-5) during the hard state, we have 145 data points which give a false alarm probability of 8×10^{-6}.

Wilms et al. also fit the pointed RXTE observations to two Comptonization models, one based on Titarchuk (1994) and another based on Coppi (1999). The orbital variations in $N_{\rm H}$ and F(5-10)/F(2-5) are not as significant using fits with either of these models compared with the fits using the broken power law model.

The RXTE pointed observations have much higher spectral resolution, timing resolution, and sensitivity compared with the ASM observations. Here we have shown the orbital variation in absorbing column using not just broad-band colors, but detailed fits to spectra.

4. X-ray Absorption Models

From the increased X-ray absorption near $\phi = 0$ during both the soft states (§3.1) and hard states (§3.3), we can test models of how the stellar wind may change, if at all, between those states.

First we assume that the stellar wind is identical during the soft and hard states, and that the only change is in the X-ray spectrum ionizing the wind. We compute the ionization in the stellar wind in response to X-ray illumination by the soft or hard state X-ray spectrum. Then we examine the limits of wind mass loss rate and terminal velocity

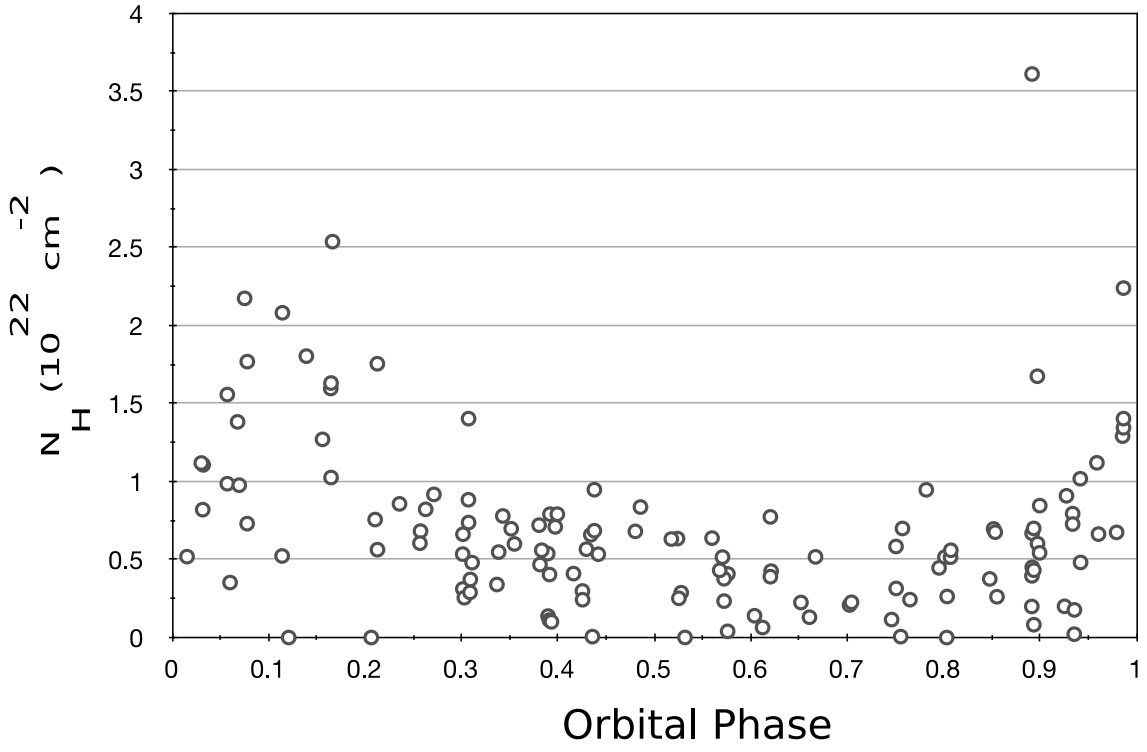

Fig. 11.— We plot versus orbital phase the values of $N_{\rm H}$, the hydrogen column density, from fits of broken power law models to RXTE pointed observations of Cygnus X-1 detailed in Wilms et al. 2006

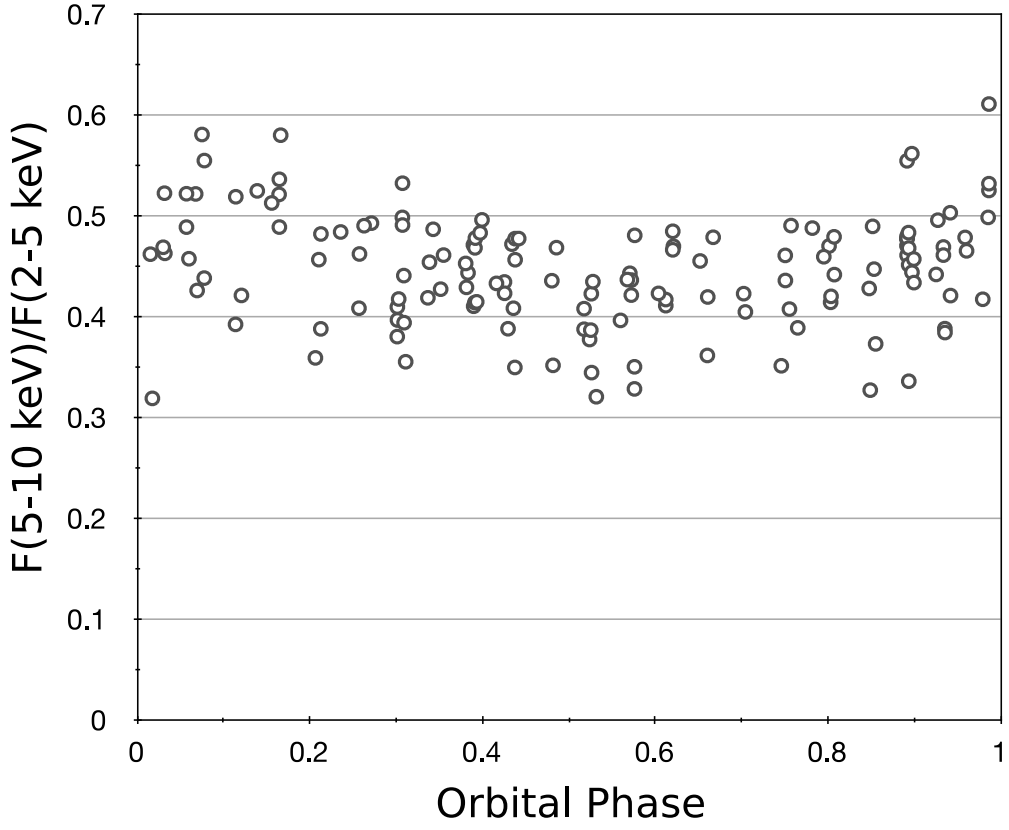

Fig. 12.— Phase variability of $F(5-10)/F(2-5)$, the ratio of fluxes in the 5–10 keV band to the 2–5 keV band, from fits to the pointed RXTE observations presented by Wilms et al. 2006. The fits assume a broken power law model.

that are compatible with orbital variability in each state.

4.1. Input X-ray Spectrum

The ionization in the stellar wind depends on the X-ray spectrum. To compute the ionization in the wind, we use the XSTAR program (Bautista & Kallman, 2001). Under the assumption that the wind is optically thin to the X-rays from the vicinity of the black hole, the ionization and temperature equilibria can be computed based on the ionization parameter $\xi = L/nr^2$ where L is the X-ray luminosity, n is the hydrogen density, and r is the distance to the X-ray source.

XSTAR requires as input the luminosity L in the 13.6 eV to 13.6 keV range. Extending the power law to low energies, particularly during the soft state, would lead to an unrealistic spectrum. We model the spectrum using the Bulk Motion Comptonization (BMC) model (Shaposhnikov & Titarchuk 2007), which has been implemented in the XSPEC spectral fitting program. This model provides a physically-motivated spectrum that is similar to a blackbody and a broken power law.

However, there may be an additional soft blackbody component with $kT \sim 0.1-0.2$ keV, as observed by Ebisawa et al. (1996) with ASCA.

We therefore simulate the orbital variability in X-ray absorption using spectra given by the BMC fits of Shaposhnikov & Titarchuk (2007) with or without an added soft blackbody component of $kT = 0.1$ keV. We present here only the results without the soft blackbody, which has a greater effect on the UV P Cygni lines than on the X-ray absorption. For each model we identify both the 13.6 eV to 13.6 keV luminosity, which is what XSTAR requires, and the 2-200 keV X-ray luminosity, which describes the X-ray output in the range observed by RXTE.

4.2. Smooth, Partially Ionized Wind Absorption Model

We make a model similar to that of Wen et al. (1999), in which the orbital variation of X-rays results from the black hole passing behind larger column densities of partially ionized wind near $\phi = 0$.

We fix the orbital inclination to 30 degrees, the radius of the O star to R_O =1.387×10^{12} cm, and the orbital separation to 2 R_O. We fix the radial velocity law in the wind to be $v(R) = 1430(1 - R_O/R)^\beta$ with $\beta = 0.75$. The wind parameters are based on the fits to the UV P Cygni lines observed during the X-ray soft state with the HST *STIS*, as reported in Vrtilek et al. (2008).

We calculate, in phase intervals of $\Delta\phi = 0.05$, the column density of the sight line to the black hole at each ionization parameter between $\log \xi = 1$ and $\log \xi = 5$. This quantity, $N(\phi, \log \xi)$, can be adjusted for various values of the wind mass loss rate $\dot{M}$ and the X-ray luminosity L_x, by

$$N'(\phi, \log \xi) = \frac{\dot{M}'}{\dot{M}} N(\phi, \log \frac{L_x \dot{M}'}{L'_x \dot{M}} \xi) \tag{1}$$

where $\dot{M}$ and L_x have been changed to take on values $\dot{M}'$ and L'_x respectively.

From XSTAR, we calculate the transmission of the source spectrum as it passes through each column at each value of $\log \xi$, and thus the X-ray spectrum at each phase ϕ. We add the Compton scattering column density to the photoabsorption column predicted by XSTAR. This allows us to find those values of $\dot{M}$ and L_x that predict the orbital variation in the Cyg X-1 X-ray spectrum that results entirely from the black hole's motion through a smooth, partially ionized stellar wind.

The results of fitting the model to the orbital variation are shown in Table 2. The best-fit values provided for $\dot{M}$ and L_x are uncertain, as these parameters vary in tandem. The contours of reduced χ^2 provide a measure of which ranges of $\dot{M}$ and L_x are acceptable,

although the models only provide fits with $\chi^2_\nu \approx 1$ for HR1 during the Soft 3 state. In the hard state, the models strongly favor $L_{\rm x,37}/\dot{M}_{-6} < 1$, $\dot{M}_{-6} < 4$, while in the soft state, they favor $L_{\rm x,37}/\dot{M}_{-6} < 1.5$ and $\dot{M}_{-6} < 2$, where we use $L_{\rm x,37} \equiv L_{\rm x} \times 10^{-37}$ erg s^{-1} and $\dot{M}_{-6} \equiv \dot{M} \times 10^6 M_\odot$ yr^{-1}. For the soft state, the χ^2 contours given by fits to the HR1 color and to the individual X-ray bands are complementary, limiting $L_x/\dot{M}$ and $\dot{M}$, respectively.

4.3. Cold Wind Clump Absorption Model

The discrete X-ray dips seen in Cyg X-1, particularly near $\phi = 0$ (Balucińska-Church et al. 2000), may be related to the dips seen in such X-ray binaries as Hercules X-1 (e.g. Shakura, Prokhorov, Postnov, & Ketsaris 1999), or the class known as "dippers" (Frank, King, & Lasota 1987). In these systems, dips may be associated with the gas stream feeding the accretion disk through Roche lobe overflow. The focused wind in Cyg X-1 could provide a similar absorbing structure. However, a full treatment of a focused wind would be beyond the scope of this paper, and would probably require hydrodynamic modeling.

Instead of dealing with complex asphericity, we pursue an alternative to the smooth, partially ionized wind model in which the wind is still assumed to be spherically symmetric and the orbital variation in the X-ray spectrum still results from the line of sight at $\phi = 0$ passing through more of the dense wind regions. However, we assume that the absorption is caused by neutral clumps, and that the chance of such a clump passing through the line of sight is linearly proportional to the wind column density. We fix the clump column density to $N_H = 4 \times 10^{22}$ cm^{-2}, following the ASCA observations of X-ray dips (Ebisawa et al. 1996). We allow two free parameters, the covering fraction of the clump when the wind column density reaches its maximum, and the mass-loss rate in the wind. The latter influences the X-rays only through Compton scattering, as the wind outside of the dense clumps is entirely ionized. The results do not constrain $\dot{M}$ very well, although at too high

values, too great an orbital variation is seen. The covering fraction parameter serves as a time-average of the actual covering fraction during dips with the zero covering fraction in periods when dips are not present.

4.3.1. Hard State

We first fit the model to the ASM light curves in the 1.5–3, 3–5, and 5–10 keV bands during the hard state. We define the hard state as the entire light curve excluding the soft states identified in Table 1. This may include some "failed transistions" to the soft state, or intermediate states.

The best-fit values for the smooth wind model are $\dot{M} \approx 2 \times 10^{-6}$ $M_\odot$ yr^{-1} and $L_x \approx 2 \times 10^{37}$ erg s^{-1}. For the computation of χ^2_ν, we use errors for the binned light curve based on the variance within each bin.

We also try fits to the hardness ratio HR1 (flux in the 3–5 keV band divided by flux in the 1.5–3 keV band).

For the hard state, the dense clump model using partial covering and the smooth partially ionized wind model fit the data equally well.

4.3.2. Soft State

We apply again the model of absorption in a partially ionized smooth wind but now to the "Soft 3" period. The strong orbital variation in HR1 is better explained by a neutral absorber than by a smooth partially ionized wind. The values of $\dot{M}$ and L_x which provide the best fit to the variations in 1.5–3, 3–5, and 5–10 keV bands predict a 3.6% peak to peak variation in HR1, whereas an 11% variation is actually observed. A neutral absorber would

absorb most strongly the soft X-rays, thus increasing the variation in HR1.

For the neutral clump model, the free parameters are the covering fraction and $\dot{M}$ in the fully ionized remainder of the wind, which affects the fit only through the variable column for Compton scattering. For the 1.5–3, 3–5, and 5–10 keV bands, we obtain $\chi^2_\nu = 3.3$ at a covering fraction of 0.14, while for HR1 we obtain $\chi^2_\nu = 0.9$ at a covering fraction of 0.28. The larger covering fraction required to fit the hardness ratio is consistent with the hardness ratio giving a wider variation than expected from the variation in the individual bands. That the covering fractions differ in the fits to the individual energy bands and to the hardness ratio may indicate a deficiency in the model. The χ^2_ν values for the partial covering neutral clump model are comparable but slightly superior to the χ^2_ν values for the smooth partially ionized wind absorption model.

5. Discussion

We are able to set some broad limits on how the mass-loss rate and X-ray luminosity may vary between the hard and soft states. Consistent with the earlier results of Gies et al. (2003), the limit that we have set on the wind mass-loss rate in the Soft state ($\dot{M}_{-6} < 2$) is lower than the limit on the mass-loss rate in the Hard state ($\dot{M}_{-6} < 4$). However, the models make many simplifications and the wind in Cyg X-1 is probably complex and aspherical.

The X-ray dips seen in Cyg X-1 may be caused by high density regions of the wind passing through the line of sight. The wind density could be increased locally from some interaction between the wind and the compact object or globally from instabilities common to the radiative acceleration of O star winds. Density contrasts of $\sim 10^3$ are commonly seen in simulations of O star wind acceleration (Owocki, Castor, & Rybicki 1988). From

the duration of the observed dips, $\Delta\phi \lesssim 0.005 \sim 200$s, the clumps would have linear size $\sim 10^{10}$ cm, given that the compact object moves with velocity 360 km s^{-1} and wind velocities are typically ~ 1000 km s^{-1}.

For a density contrast of 10^3, a typical spherical region of radius 10^{11} cm would contain one absorbing clump of radius 10^{10} cm. We assume that the wind outside of the clump does not contribute to absorbing dips. There would be ~ 10 absorbing clumps within a stellar radius, each clump presenting ~ 0.01 of the surface area of the surrounding 10^{11} cm radius sphere. Thus we would expect a clump covering fraction of ~ 0.1, which is consistent with the results of the simple models shown in Table 2.

It has been suggested (Kaper et al. 1993) that the flares seen in some accreting binaries result from accretion of inhomogeneities in the stellar wind. If, as suggested above, a typical clump has radius 10^{10} cm and is overdense by a factor of $\sim 10^3$, then it will provide a mass of $\sim 10^{20}$ g. With an accretion efficiency of 0.1, this would provide a luminosity of $\sim 10^{38}$ erg s^{-1} over a period of 100 s, consistent with observed flares. However, this analysis does not explain the dependence of flaring on X-ray state. Our suggestion that the wind mass-loss rate $\dot{M}$ is greater during the hard-low state appears to be inconsistent with increased flaring during the soft-high state. Ducci et al. (2009) modeled the accretion of clumps in the winds of supergiant High Mass X-ray binaries and showed that a greater $\dot{M}$ should lead to brighter flares. However, the flares also depend on the distribution of clump size, as well as other wind parameters that may change between the two states.

If a focused wind is present and resolved into clumps with the parameters we have described, there may be observable implications for the UV P Cygni lines. The clump covering fraction for the O star may be less than that for the black hole as a result of the orbital inclination. Whereas the wind outside of the clumps will be mostly ionized to stages higher than N V and Si IV by X-ray illumination, we expect that most of the N in the

clumps will be at lower ionization stages than N V, as the higher density will reduce $\log \xi$ by 3. As a result, the clumps may not contribute to the profiles of the N V $\lambda\lambda$ 1238.8, 1242.8 doublet. However, Si IV may be the dominant ionization stage of Si in the clumps, and thus an absorption component of depth $\lesssim 5\%$, limited by the covering fraction, could persist at $\phi = 0.5$ in the Si IV $\lambda\lambda$ 1393.7, 1402.8 doublet. Such an absorption feature varying between hard and soft states could not be ruled out by present UV observations.

In some models of the Superfast X-ray Transients (SFXTs, Sguera et al. 2005), a new class of X-ray source discovered with INTEGRAL, accretion of clumps from an OB star wind play an important role (Walter & Zurita Heras 2007). The study of absorption dips reported here complements the active research on SFXTs, whose compact objects may accrete from stellar winds at greater orbital distances.

Results provided by the ASM/RXTE teams at MIT and at the RXTE SOF and GOF at NASA's GSFC.

This paper benefited from discussions with Jeff McClintock and Jan Vrtilek.

Table 1. Starting and ending MJD defining the Cyg X-1 soft states referred to in the text.

Label	Start (MJD)	Stop (MJD)	Duration (d)
Soft 1	50,220	50,300	200
Soft 2	51,850	51,950	50
Soft 3	52,165	52,555	390
Soft 4	52,800	52,850	100
Soft 5	53,275	53,475	80

Table 2. Model fits to the Cyg X-1 variability in three RXTE ASM energy bands or to the hardness ratio between the two low energy bands. We give here the X-ray luminosity L_x and wind mass-loss rate $\dot{M}$ of the best fit.

State	Data	Model	χ^2_ν	$L_x/10^{37}$ (erg s^{-1})	$\dot{M} \times 10^6$ ($M_\odot$ yr^{-1})	F_c [a]
Soft	1.5–3, 3–5, 5–10 keV	Smooth wind	3.5	0.25	0.36	NA
Soft	1.5–3, 3–5, 5–10 keV	Partial covering	3.3	NA	NA	0.14
Soft	3–5 keV / 1.5–3 keV	Smooth wind	1.10	0.25	0.72	NA
Soft	3–5 keV / 1.5–3 keV	Partial covering	0.9	NA	NA	0.28
Hard	1.5–3, 3–5, 5–10 keV	Smooth wind	3.2	1.7	1.8	NA
Hard	1.5–3, 3–5, 5–10 keV	Partial covering	3.1	NA	NA	0.30
Hard	3–5 keV / 1.5–3 keV	Smooth wind	2.8	1.5	2.2	NA
Hard	3–5 keV / 1.5–3 keV	Partial covering	2.6	NA	NA	0.30

[a]Covering fraction

REFERENCES

Balucińska-Church, M., Church, M.J., Charles, P.A., Nagase, F., LaSala, J., & Barnard, R. 2000, MNRAS, 311, 861

Bautista, M.A., & Kallman, T.R. 2001, ApJS, 134, 139

Bolton, C.T. 1972, Nature, 235, 271

Bradt, H.V., Rothschild, R.E., & Swank, J.H. 1993, A&AS, 97, 355

Brocksopp, C., Fender, R.P., Larinov, V., Lyuty, V.M., Tarasov, A.E., Pooley, G.G., Paciesas, W.S., & Roche, P. 1999a, MNRAS, 309, 1063

Brocksopp, C., Tarasov, A.E., Lyuty, V.M., & Roche, P. 1999b, A&A, 343, 861

Caballero-Nieves, S.M., Gies, D.R., Bolton, C.T., Hadrava, P., Herrero, A., Hillwig, T.C., Howell, S.B., Huang, W., Kaper, L., Koubský, & McSwain, M.V. 2009, ApJ, 701, 1895

Coppi, P. in High Energy Processes in Accreting Black Holes, ed. J. Poutanen & R. Svensson, 1999, Astron. Soc. Pacific Conf. Ser. No. 161 (San Franscisco: Astron. Soc. Pacific), 375

Davies, S.R. 1991, MNRAS, 251, 64P

Dong, A., Wang, J., & Xue, L. 2007, Chinese Astronomy and Astrophysics, 31, 21

Ducci, L, Sidoli, L, Mereghetti, S., Paizis, A., & Romano, P. 2009, MNRAS, submitted

Dupree, A.K., Davis, R.J., Gursky, H., Hartmann, L.W., Raymond, J.C., Boggess, A., Holm, A., Kondo, Y., Wu, C.-C., Maccheto, F., Sandford, M.C.W., Willis A.J., Wilson, R., Ciatti, F., Hutchings, J.B., Johnson, H.M., Perinotto, M., & Whittet, D.C.B. 1978, Nature, 275, 400

Ebisawa, K., Ueda, Y., Inoue, H., Tanaka, Y., & White, N.E. 1996, ApJ, 467, 419

Feng, Y.X., & Cui, W. 2002, ApJ, 564, 953

Frank, J., King, A.R., & Lasota, J.-P. 1987, A&A, 178, 137

Gies, D.R., Dieterich, S., Richardson, N.D., Riedel, A.R., Team, B.L., McAlister, H.A., Bagnuolo, W.G., Jr., Grundstrom, E.D., Štefl, S., Rivinius, Th., Baade, D. 2008, ApJ, 682, 117

Gies, D.R., Bolton, C.T., Thomson, J.R., Huang, W., McSwain, M.V., Riddle, R.L., Wang, Z., Wiita, P.J., Wingert, D.W., Csák, B., Kiss, L.L. 2003, ApJ, 583, 424

Grebenev, S., Sunyaev, R., Pavlinsky, M., Churazov, E., Gilfanov, M., Dyachkov, A., et al. 1993, A&AS, 97, 281

Grove, J.E., Johnson, W.N., Kroeger, R.A., McNaron-Brown, K., & Skibo, J.G. 1998, ApJ, 500, 899

Hanke, M., Wilms, J., Nowak, M.A., Pottschmidt, K., Schulz, N.S., & Lee, J.C. 2009, ApJ, 690, 330

Hatchett, S., & McCray, R. 1977, ApJ, 211, 552

Herrero, A., Kudritzki, R.P., Gabler, R., Vilchez, J.M., & Gabler, A. 1995, A&A, 297, 556

Holt, S.S., Kaluzienski, L.J., Boldt, E.A., & Serlemitsos, P.J. 1979, ApJ, 233, 344

Ibragimov, A., Zdiarski, A.A., Poutanen, J. 2007, MNRAS, 381, 723

Jahoda, K., Swank, J.H., Giles, A. B., Stark, M. J., Strohmayer, T., Zhang, W., & Morgan, E. H. 1996, SPIE, 2808, 59J

Kaper, L., Hammerschlag-Hensberge, G., & van Loon, J.T. 1993, A&A, 279, 485

Lachowicz, P., Zdiarski, A.A., Schwarzenberg-Czerny, A., Pooley, G.G., & Kitamoto, S. 2006, MNRAS, 368, 1025

Levine, A.M., Bradt, H., Cui, W., Jernigan, J.G., Morgan, E.H., Remillard, R., Shirey, R.E., & Smith, D.A. 1986, ApJ, 460, L33

Marshall, H.L., et al. 2001, in Proc. Joint Workshop on X-ray Emission from Accretion onto Black Holes, ed. T. Yaqoob & J. Krolik, preprint (astro-ph/0111464)

Mason, K.O., Hakins, F.J., Sanford, P.W., Murdin, P., & Savage, A. 1974, ApJ, 192, 65

Owocki, S.P., Castor, J.I., & Rybicki, G.B. 1988, ApJ, 335, 914

Priedhorsky, W.C., Brandt, S., & Lund, N. 1995, A&A, 300, 415

Remillard, R.A., & McClintock, J.E. 2006, ARA&A, 44, 49

Rothschild, R. E., Blanco, P. R., Gruber, D. E., Heindl, W. A., MacDonald, D. R., Marsden, D. C., Pelling, M. R., Wayne, L. R., Hink, P. L. 1998, ApJ, 496, 538

Scargle, J.D. 1982, ApJ, 263, 835

Schulz, N.S., Cui, W., Canizares, C.R., Marshall, H.L., Lee, J.C., Miller, J.M., & Lewin, W.H.G. 2002, ApJ, 565

Sguera, V., Barlow, E.J., Bird, A.J., et al. 2005 A&A, 444, 221

Shakura, N.I., Prokhorov, M.E., Postnov, K.A., & Ketsaris, N.A. 1999, A&A, 348, 917

Shaposhnikov, N., & Titarchuk, L. 2007, ApJ, 663, 445

Tarasov, A.E., Brocksopp, C., & Lyuty, V.M. 2003, A&A, 402, 237

Titarchuk, L. 1994, ApJ, 434, 570

Treves, A., Chiappetti, L, Tanzi, E.G., Tarenghi, M., Gursky, H., Dupree, A.K., Hartmann, L.W., Raymond, J., Davis, R.J., Black, J. 1980, ApJ, 242, 1114

van Loon, J.Th., Kaper, L., & Hammerschlag-Hensberge, G. 2001, A&A 375, 498

Vrtilek, S.D., Boroson, B., Hunacek, A., Gies, D., & Bolton, C.T. 2008, ApJ, 678, 1248

Walter, R., & Zurita Heras, J. 2007, A&A, 476, 335

Wen, L., Cui, W., Levine, A.M., & Bradt, H.V. 1999, ApJ, 525, 968

Wilms, J., Nowak, M.A., Pottschmidt, K., Pooley, G.G., & Fritz, S. 2006, A&A, 447, 245

Ziólkowski, J. 2005, MNRAS 358, 851

This manuscript was prepared with the AAS LaTeX macros v5.2.